frontiers in Physics

ORIGINAL RESEARCH
published: 22 February 2021
doi: 10.3389/fphy.2020.616790

Development of Dynamic Model and Analytical Analysis for the Diffusion of Different Species in Non-Newtonian Nanofluid Swirling Flow

Auwalu Hamisu Usman[1,2], *Noor Saeed Khan*[1,3,4,5]*, *Usa Wannasingha Humphries*[1]*, *Zahir Shah*[4,6], *Poom Kumam*[1,3,4,7]*, *Waris Khan*[8], *Amir Khan*[9], *Sadiya Ali Rano*[2] and *Zafar Ullah*[5]

[1]Department of Mathematics, Faculty of Science, King Mongkut's University of Technology Thonburi (KMUTT), Bangkok, Thailand, [2]Department of Mathematical Sciences, Bayero University, Kano, Nigeria, [3]KMUTT-Fixed Point Theory and Applications Research Group, Theoretical and Computational Science Center (TaCS), Science Laboratory Building, Faculty of Science, King Mongkut's University of Technology Thonburi (KMUTT), Bangkok, Thailand, [4]Center of Excellence in Theoretical and Computational Science (TaCS-CoE), SCL 802 Fixed Point Laboratory, Science Laboratory Building, King Mongkut's University of Technology Thonburi (KMUTT), Bangkok, Thailand, [5]Division of Science and Technology, Department of Mathematics, University of Education Lahore, Lahore, Pakistan, [6]Department of Mathematics, University of Lakki Marwat, Lakki Marwat, Pakistan, [7]Department of Medical Research, China Medical University Hospital, China Medical University, Taichung, Taiwan, [8]Department of Mathematics and Statistics, Hazara University Mansehra, Khyber Pakhtunkhwa, Pakistan, [9]Department of Mathematics and Statistics, University of Swat, Khyber Pakhtunkhwa, Pakistan

OPEN ACCESS

Edited by:
Antonio F. Miguel,
University of Evora, Portugal

Reviewed by:
Latif Ahmad,
Shaheed Benazir Bhutto University, Pakistan
Eda Aydin,
Ontario Tech University, Canada
Jawad Ahmed,
University of Engineering and Technology, Pakistan

***Correspondence:**
Usa Wannasingha Humphries
usa.wan@kmutt.ac.th
Noor Saeed Khan
noorsaeedkhankhattak@gmail.com
Poom Kumam
poom.kum@kmutt.ac.th

Specialty section:
This article was submitted to Interdisciplinary Physics, a section of the journal Frontiers in Physics

Received: 13 October 2020
Accepted: 23 December 2020
Published: 22 February 2021

Citation:
Usman AH, Khan NS, Humphries UW, Shah Z, Kumam P, Khan W, Khan A, Rano SA and Ullah Z (2021) Development of Dynamic Model and Analytical Analysis for the Diffusion of Different Species in Non-Newtonian Nanofluid Swirling Flow. Front. Phys. 8:616790. doi: 10.3389/fphy.2020.616790

The analysis is carried out to analyze the flow through double stretchable rotating disks with the theory of radiative Cross nanofluid under the influence of variable thermal conductivity, the Hall current, Arrhenius activation energy, and binary chemical reactions. The Buongiorno nanofluid model is adopted for the governing equations of the problem which are transformed into ordinary differential equations through similarity transformations and then solved using the homotopy analysis method. The impact of dimensionless parameters on all profiles and physical quantities is presented and discussed. The radial velocity of the two disks increases with their corresponding ratio stretching rate parameter and decreases with the Hall parameter and the bioconvection Rayleigh number. The heat transfer at the lower disk enhances with the variable thermal conductivity parameter, while at the upper disk, opposite trend is observed. Mass transfer increases with the chemical reactions and temperature difference parameters at the lower disk and decreases with Arrhenius activation energy, whereas an opposite trend is observed at the upper disk. The local density number is enhanced for the larger values of Peclet and Lewis numbers. The comparison of the present work with the published literature authenticates the validation of the present work.

Keywords: nanofluid, nanofluid (Buongiorno model), heat transfer, gyrotactic microorganism, rotating/stretching surface

INTRODUCTION

Cross [1] carried out an innovative work on the Cross model in 1965. Cross fluid is a separate generalization of non-Newtonian fluid types, which has served as a model offering a wide range of shearing rates for the dilatant and pseudoplastic origin of the fluids. A variety of applications involves polymerization in the Cross-fluid model. Xie and Jin [2] reported a Cross rheological equation analysis for the surface free layer of non-Newtonian fluid. Manzur et al. [3] studied the Cross-fluid model with flow through the extended vertical sheet stretching layer by examining the mixed convection and radiative heat transfer. Abbas et al. [4] considered the Cross nanofluid flow subject to entropy generation mathematical modeling and analysis. Hayat et al. [5] performed a numeric simulation of MHD stagnation of Cross-fluid model flow and heat transfer in a stretched surface. Naz et al. [6] studied the Cross nanofluid dynamics with magnetohydrodynamics, entropy, and gyrotactic motile microbiological characteristics.

The thermal transformation process is characterized by the thermal conductivity of the basic fluid due to poor thermal conductivity of nonmetallic materials such as mud, oils, and glycol mixture in contrast to some metallic materials like copper, aluminum, iron, bronze, etc. The properties of low thermal-conducting nanoparticles, usually made up of oxides and metals, significantly increase the base fluid thermal conductivity. The conductivity and convection coefficients of metals and oxides increase the efficiency of heat transfer in nanofluids. Choi and Eastman [7] in 1995 first suggested the term "nanofluid" by using very small (1–100 nm) nanoparticles added to the base fluid. Boungiorno [8] suggested the slips mechanisms like inertia, dissipation, magnus, fluid drainage, gravity, Brownian diffusion, and thermophoresis effects in the dynamics of nanofluids. Kuznetsov and Nield [9] used the Buongiorno model to address the nanoparticles' effects on natural convective boundary flow *via* a vertical plate. The main work focusing on normal cases using nanofluids for all purposes began in 1995 with Choi and Eastman on their study to assign the suspension of solid nanoparticles to the base fluid, where they found that the thermal conductivity of the water–Al_2O_3 blend was increased by 20% for a concentration of the volumes in the range of 1–5% of Al_2O_3. Turkyilmazoglu [10] reported the study of nanofluid flow and heat transfer due to a rotating disk. Ahmad et al. [11] presented a numerical study of generalized non-Newtonian unsteady 3D magneto-nanoparticles liquid flow. Hafeez et al. [12] investigated the rotational flow of Oldroyd-B nanofluid under Cattaneo–Christov double diffusion theory. Khan et al. [13] reported a 3D numerical unsteady Sisko magneto-nanofluid flow study with heat absorption and temperature-dependent thermal conductivity. More nanofluid studies can be found in Refs. 14–21.

Bioconvective phenomena are common in suspension, usually due to the swimming of microorganisms that are marginally denser than water. If the upper surface of the suspension is too thick due to the accumulation of microorganisms, it becomes brittle and the microorganisms collapse to induce the bioconvection. The development of gyrotactic nanofluid microorganisms enables mass transfer, microscale mixing, primarily in microvolumes, and improves nanofluid stability. Li and Xu [22] studied the unsteady mixed bioconvection flow of a nanofluid between two contracting or expanding rotating disks. Qayyum et al. [23] examined the analysis of radiation in a suspension of nanoparticles and gyrotactic microorganism for rotating disk of variable thickness. Shehzad et al. [24] investigated the Maxwell nanofluid bioconvection on isolated rotating disks under the influence of the double-diffusive Cattaneo–Christov theory. Khan et al. [25] reported the study of entropy generation in bioconvection nanofluid flow between two stretchable rotating disks. More studies on bioconvection can be found in Refs. 26–30.

Scientists and engineers, particularly in the areas of oil, chemical and petroleum engineering, oil and water emulsion, cooling reactors, geothermal, mechanical chemistry, and material degradation, have been very interested in multi-specific applications such as energy activation and species response. Generally, the relation between chemical reactions and mass transfer is highly complex and can only be studied by producing and digesting reagent species at different fluid flow and mass transfer rates. Arrhenius [31] for the first time suggested the concept of activation energy. However, Bestman [32] recognized a principal model of a boundary layer of flow problem due to binary chemical reactions with Arrhenius activation energy. Shahzad et al. [33] investigated the transport of radiative heat transfer with entropy generation and activation energy in dissipative nanofluid flow. Dhlamini et al. [34] suggested the mixed convective nanofluid flow with convective boundary conditions under binary chemical reaction and Arrhenius activation energy. Azam et al. [35] investigated the Arrhenius activation energy effects on radiative Cross-nanofluid axisymmetric flow through covalent bonding development. More studies on Arrhenius activation energy and binary chemical reaction can be seen in Refs. 36–40.

The idea of flow into a rotating disk system is an important area for future industrial process optimization and development. Scientists all over the world have drawn attention to this idea with the applications in the fields of electrochemistry, energy engineering, aerodynamics, chemical engineering, food processing, and medical equipment. To the best of knowledge, Karman [41] initially investigated the flow of liquid through an infinite disk with the introduction of famous similarity transformations in his study. Hayat et al. [42] investigated the viscous dissipation in the second-grade fluid flow in rotating disk with the Joule heating. Yao and Lian [43] reported the flow due to rotation, in which they provided analytical and numerical solutions when the fluid is rigidly rotated. Hayat et al. [44] investigated the flow between two stretchable rotating disks with the Cattaneo–Christov heat flux model. More studies on a rotating disk system can be consulted in Refs. 45 and 46.

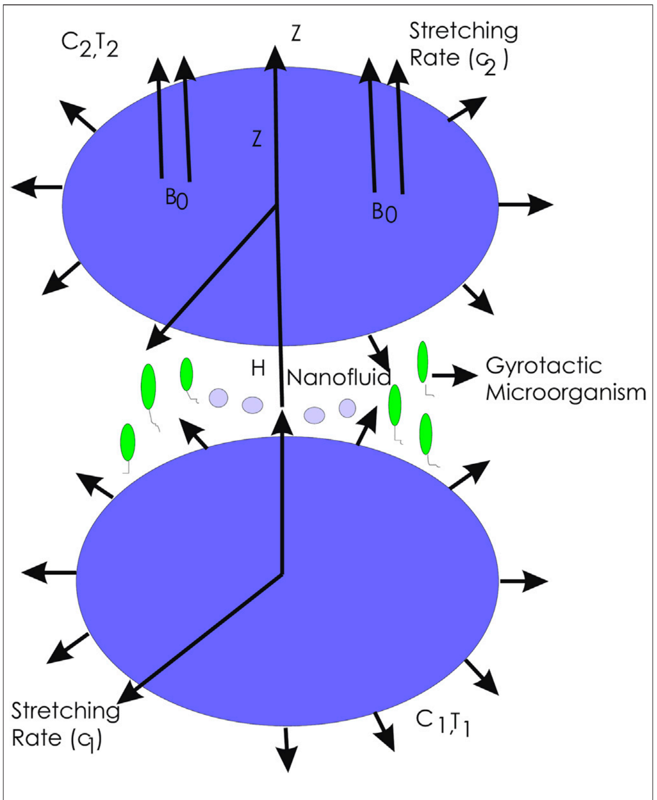

FIGURE 1 | Geometry of the problem.

In the light of the abovementioned literature, no one has, to the best of our knowledge, studied the flow between two stretchable rotating disks under the radiative Cross-nanofluid theory in the following context. The objective, here is, to explore the flow of Cross nanofluid in the presence of variable thermal conductivity, the Hall effect, and Arrhenius activation energy effect. The Buongiorno nanofluid model is used to develop Brownian diffusion and thermophoresis effects in both the energy and concentration equations. The problem is solved through HAM [47, 48] presented by Liao in 1992. However, due to its rapid convergence, various researchers [49–74] used HAM and various potential techniques to solve their problems. The effects of the parameters on the profiles are explained through graphs and tables whose detail is given in the *Discussion* section.

PROBLEM FORMULATION

A three-dimensional, steady, axisymmetric motion of MHD flow of incompressible radiative Cross nanofluid through rotating double disks is considered. The lower disk is at the plane $z = 0$. Fluid motion is subjected to rotation in axial direction of the disks having amplitude ε_o and angular velocities γ_1 and γ_2 lower and upper disks, respectively. Investigations are made by considering cylindrical coordinates. The velocity components (u, v, w) along the directions of (r, ϑ, z), respectively. Let (T_1, T_2) indicate the constant temperatures prescribed for both the low and upper disks where $T_1 > T_2$, and the concentrations in the lower and upper disks are represented by (C_1, C_2). By regarding the flow to be axisymmetric, thus, the tangential coordinate derivatives with respect to ϑ are omitted. The magnetic field B_o with uniform intensity acts in the axial direction. Furthermore, due to the low Reynolds number, the induced magnetic field is zero, and there is also an exclusion of the electrical field. Nanofluid dilution to consider viscosity dispersion is used to prevent bioconvection instability. The nanoparticles suspended in the base fluid are also expected to be stable so that they do not affect the swimming pathway and the velocity of the microorganisms. N_1 and N_2 are the motile gyrotactic microorganism distributions on the lower and upper disks, respectively. **Figure 1** shows the physical form of the problem. The guiding principles are the governing equations that follow the Buongiorno nanofluid model.

The Hall current is influencing many fields such as medical sciences and engineering. Cosmological fluid dynamics, geophysics, and the Hall accelerator can be listed as various engineering applications of the Hall current. The Hall current is induced by the significantly strong magnetic field. Generalized form of Ohm's law in the existence of the electric fields is given by

$$J + \frac{\sigma\mu_e}{B_o}(J \times B) = \sigma\left[\mu_e V \times B + \frac{1}{en_e}\nabla p_e\right], \tag{1}$$

assuming that the thermoelectric pressure and ion slip conditions for weakly ionized gas are negligible. Hence, the equations reduced in the form as

$$J_r = \frac{\sigma\mu_e B_o}{1+m^2}(mv - u) \text{ and } J_z = \frac{\sigma\mu_e B_o}{1+m^2}(mu + v), \tag{2}$$

where ω_e is the electron's cyclotron frequency, e is the electron collision time, p_e is the pressure of the electron, n_e is the electron's density number, μ_e is the magnetic permeability, and σ is the electrical conductivity of fluid. The Hall parameter here is defined as $m = \omega_e\tau_e$.

The Cauchy stress tensor (Cross-viscosity model) is displayed as

$$\tau = -pI + \mu(\dot{\gamma})A_1, \tag{3}$$

where μ is the viscosity, I is the identity matrix, p is the pressure, and A_1 is the first Rivlin–Ericksen tensor given as

$$A_1 = \nabla V + (\nabla V)^T, \tag{4}$$

where ∇V stands for the velocity gradient. For generalized Newtonian fluid subclass (Cross fluid), the viscosity rheology equation is

$$\mu = \mu_\infty + \frac{\mu_o - \mu_\infty}{1 + (\Gamma\dot{\gamma})^n}, \tag{5}$$

by taking viscosity infinite shear rate to zero $(\mu_\infty = 0)$, the stress tensor now becomes

$$\tau = -pI + \mu_o\left[1 + (\Gamma\dot{\gamma})^n\right]^{-1}A_1. \tag{6}$$

Taking the assumption $\Gamma = 0$, the original Newtonian model is obtained. It is apparent that the Cross fluid chooses to act as shear thinning fluid for the range $0 < n < 1$; that is, n is the power law index for Cross fluid used for choosing to behave like shear thinning in the range of 0 and 1.

The Cross-viscosity model shear rate in the existence of simulation is given as

$$\dot{\gamma} = \sqrt{\frac{1}{2}\sum_i\sum_j \dot{\gamma}_{ij}\dot{\gamma}_{ji}} = \sqrt{\frac{1}{2}tr\left(A_1^2\right)}, \tag{7}$$

where $tr\left(A_1^2\right)$ is the trace of the matrix A_1^2.

Now the continuity, momentum, energy, concentration, and gyrotactic microorganism equations [1, 3, 5, 6, 34] are

$$\frac{\partial u}{\partial r} + \frac{u}{r} + \frac{\partial w}{\partial z} = 0, \tag{8}$$

$$u\frac{\partial u}{\partial r} + w\frac{\partial u}{\partial z} - \frac{v^2}{r} = -\frac{1}{\rho_{nf}}\frac{\partial p}{\partial r} + \nu_{nf}\frac{\partial}{\partial z}\left[\frac{\left(\frac{\partial u}{\partial z}\right)}{1 + \left(\Gamma\frac{\partial u}{\partial z}\right)^n}\right] - \frac{\sigma_{nf}B_o^2}{\rho_{nf}\left(1 + m^2\right)}(u - mv)$$
$$+\frac{1}{\rho_{nf}}\left[(1 - C_2)\rho_{nf}\beta(T - T_2) - \left(\rho_p - \rho_{nf}\right)(C - C_2) - (N - N_2)\left(\rho_m - \rho_{nf}\right)\right]g, \tag{9}$$

$$u\frac{\partial v}{\partial r} + w\frac{\partial v}{\partial z} + \frac{vu}{r} = \nu_{nf}\frac{\partial}{\partial z}\left[\frac{\partial v/\partial z}{1 + (\Gamma\partial v/\partial z)^n}\right] - \frac{\sigma_{nf}B_o^2}{\rho_{nf}\left(1 + m^2\right)}(v + mu), \tag{10}$$

$$u\frac{\partial w}{\partial r} + w\frac{\partial w}{\partial z} = -\frac{1}{\rho_{nf}}\frac{\partial p}{\partial z} + \nu_{nf}\frac{\partial}{\partial z}\left[\frac{\left(\frac{\partial u}{\partial z}\right)}{1 + \left(\Gamma\frac{\partial u}{\partial z}\right)^n}\right], \tag{11}$$

$$\left(u\frac{\partial T}{\partial r} + w\frac{\partial T}{\partial z}\right) = \frac{\mu_o}{\left(\rho c_p\right)_{nf}}\left[\frac{\left(\frac{\partial u}{\partial z}\right)^2}{1 + \left(\Gamma\left(\frac{\partial u}{\partial z}\right)^n\right)}\right]$$
$$+\left[\frac{K(T)}{r}\frac{\partial T}{\partial r} + \frac{\partial}{\partial r}\left[K(T)\frac{\partial T}{\partial r}\right] + \frac{\partial}{\partial z}\left[\left(K(T)\frac{\partial T}{\partial z}\right)\right]\right] +$$
$$\tau\left\langle D_B\left\{\frac{\partial T}{\partial z}\frac{\partial C}{\partial z} + \frac{\partial T}{\partial r}\frac{\partial C}{\partial r} + \frac{D_T}{T_2}\left[\left(\frac{\partial T}{\partial z}\right)^2 + \left(\frac{\partial T}{\partial r}\right)^2\right]\right\}\right\rangle \tag{12}$$
$$+\frac{\sigma_{nf}B_o^2\left(v^2 + u^2\right)}{\left(\rho c_p\right)_{nf}} - \frac{1}{\left(\rho c_p\right)_{nf}}\frac{\partial\left(rq_r\right)}{\partial r},$$

$$u\frac{\partial C}{\partial r} + w\frac{\partial C}{\partial z} = D_B\left(\frac{\partial^2 C}{\partial r^2} + \frac{1}{r}\frac{\partial C}{\partial r} + \frac{\partial^2 C}{\partial z^2}\right) + \frac{D_T}{T_2}\left(\frac{\partial^2 T}{\partial r^2} + \frac{1}{r}\frac{\partial T}{\partial r} + \frac{\partial^2 T}{\partial z^2}\right)$$
$$-k_r^2(C - C_2)\left(\frac{T}{T_2}\right)^{m_1}\exp\left[\frac{-E_a}{K_1 T}\right], \tag{13}$$

$$u\frac{\partial N}{\partial r} + w\frac{\partial N}{\partial z} + \frac{bW_c}{(C_1 - C_2)}\left[\frac{\partial}{\partial z}\left(N\frac{\partial C}{\partial z}\right)\right] = D_m\left(\frac{\partial^2 N}{\partial z^2}\right), \tag{14}$$

where $K(\mathrm{T})$ denotes the variable thermal conductivity and is defined as

$$K(T) = k_{nf}\left(1 + \varepsilon\frac{T - T_2}{T_1 - T_2}\right).$$

The boundary conditions are

$$u = c_1 r,\ v = r\gamma_1,\ w = 0,\ T = T_1, C = C_1,\ N = N_1,\ at\, z = 0$$
$$u = c_2 r,\ v = r\gamma_2,\ w = 0,\ T = T_2, C = C_2,\ N = N_2,\ at\, z = H. \tag{15}$$

The following transformations are used

$$u = r\gamma_1 f'(\zeta),\ v = r\gamma_1 g(\zeta),$$
$$w = -2H\gamma_1 f(\zeta),\ \mathrm{P} = \rho_{nf}\gamma_1\nu_{nf}\left[p_o(\zeta) + \frac{r^2\varepsilon_o}{2H^2}\right], \tag{16}$$
$$\theta(\zeta) = \frac{T - T_2}{T_1 - T_2},\ \phi(\zeta) = \frac{C - C_2}{C_1 - C_2},\ \chi(\zeta) = \frac{N - N_2}{N_1 - N_2}, \zeta = \frac{z}{H}.$$

Equation 8 is satisfied through **Eq 16**, and the remaining **Eqs 9–15** provide **Eqs 17–23**, respectively, as

$$\left[1 + (1 - n)\left(Wef''\right)^n\right]f'''$$
$$-\left[1 + \left(Wef''\right)^n\right]^2\left[\begin{array}{l}\mathrm{Re}\left(f'^2 - 2ff'' - g^2\right) + \frac{\mathrm{Re}M}{\left(1 + m^2\right)}(f' - mg) + \\ \lambda(\theta - N_r\phi - R_b\chi) - \varepsilon\end{array}\right] = 0, \tag{17}$$

$$\left[1 + (1 - k)\left(Weg'\right)^n\right]g''$$
$$+\mathrm{Re}\left[\left(fg' - f'g\right) - \frac{M}{1 + m^2}\left(g + mf'\right)\right]\left[1 + \left(Wef''\right)^n\right]^2 = 0, \tag{18}$$

$$P = 4\,\mathrm{Re}ff' + \left[\frac{1 + (1 + n)\left(-2\beta_1 Wef'\right)^n}{\left[1 + \left(-2\beta_1 Wef'\right)^n\right]^2}\right] = 0, \tag{19}$$

$$\left(1 + \frac{\varepsilon - 1}{\delta} + Rd\right)\theta'' + \varepsilon\left(\theta'^2 + \theta\theta''\right)$$
$$+\mathrm{Pr}\left[\begin{array}{l}Ec\beta_2\left[\frac{f''^2}{1 + \left(Wef''\right)^n}\right] + Nb\phi'\theta' + Nt\theta^2 \\ +\mathrm{Re}Ec\left[M\left(f'^2 + g^2\right) - ff'\right]\end{array}\right]$$
$$= 0, \tag{20}$$

$$\phi'' + \frac{Nt}{Nb}\theta'' + \mathrm{Re}Scf'\phi' - Sc\sigma(1 + \delta\theta)^{m_1}\mathrm{Exp}\left(-\frac{E}{1 + \delta\theta}\right) = 0, \tag{21}$$

$$\chi'' + 2\mathrm{Re}Lef\chi' - Pe\left[\chi'\phi' + H\left(\phi'\chi + N_\delta\phi\right)\right] = 0, \tag{22}$$

with boundary conditions

$$\begin{aligned} &f(0) = 0, f'(0) = s_1,\ g(0) = 0, p(0) = 1,\ \theta(0) = 1,\ \phi(0) = 1,\ \chi(0) = 1 \\ &f(1) = 0, f'(1) = s_2,\ g(1) = \gamma,\ \theta(1) = 0,\ \phi(1) = 0,\ \chi(1) = 0, \end{aligned} \tag{23}$$

$$\begin{aligned} &\text{where} \quad We = \frac{\Gamma r \gamma_1}{H}, \quad \mathrm{Re} = \frac{H^2 \gamma_1}{\nu_{nf}}, \quad M = \frac{\sigma_{nf} B_o^2}{\rho_{nf} \gamma_1}, \\ &\lambda = \frac{(1 - C_2) g \beta (T_1 - T_2) H^2}{r \gamma_1 \nu_{nf}}, \quad s_1 = \frac{c_1}{\gamma_1}, \quad s_2 = \frac{c_2}{\gamma_2}, \\ &Nr = \frac{(\rho_p - \rho_{nf})(C_1 - C_2)}{\beta \rho_{nf} (1 - C_2)(T_1 - T_2)}, \\ &Rb = \frac{(\rho_m - \rho_{nf})(C_1 - C_2)}{\beta \rho_{nf} (1 - C_2)(T_1 - T_2)}, \quad Rd = \frac{16 \sigma^* T_2^3}{3 k^* k_{nf}}, \\ &Ec = \frac{r^2 \gamma_1^2}{(\rho c_p)_{nf} (T_1 - T_2)}, \\ &\mathrm{Pr} = \frac{\nu_{nf}}{\alpha}, \quad Nt = \frac{\tau D_T (T_1 - T_2)}{T_2 \nu_{nf}}, \quad Nb = \frac{\tau D_B (C_1 - C_2)}{\nu_{nf}}, \\ &\beta_1 = \frac{H}{r}, \quad \beta_2 = \frac{\mu_o}{(\rho c_p)_{nf}}, \quad Sc = \frac{\nu_{nf}}{D_B}, \quad \sigma = \frac{k_r^2 H^2}{\nu_{nf}} \\ &\delta = \frac{T_1 - T_2}{T_2}, \quad E = \frac{E_a}{T_2 K_1}, \quad Le = \frac{\nu_{nf}}{D_m}, \quad Pe = \frac{b W_c}{D_m}, \\ &N_\delta = \frac{N_2}{N_1 - N_2}, \quad \gamma = \frac{\gamma_2}{\gamma_1} \end{aligned} \tag{24}$$

PHYSICAL QUANTITIES

The physical quantities of interests are given below.

Skin Friction Coefficients

These are defined as

$$C_{fL} = \frac{\tau_w}{\rho_{nf} (r \gamma_1)^2} \Big|_{z=0}, \quad C_{fU} = \frac{\tau_w}{\rho_{nf} (r \gamma_2)^2} \Big|_{z=H}, \quad \text{where} \quad \tau_w = \left(\tau_{zr}^2 + \tau_{z\theta}^2 \right)^{½}. \tag{25}$$

Therefore, the skin friction coefficients for the lower and upper disks are respectively, as

$$C_{fL} = \frac{\nu_{nf}}{(r \gamma_1) H} \left\{ [f''(0)]^2 + [g'(0)]^2 \right\}^{½} = \frac{1}{\mathrm{Re}_r} \left\{ [f''(0)]^2 + [g'(0)]^2 \right\}^{½}, \tag{26}$$

$$C_{fU} = \frac{\nu_{nf}}{(r \gamma_2) H} \left\{ [f''(1)]^2 + [g'(1)]^2 \right\}^{½} = \frac{1}{\mathrm{Re}_r} \left\{ [f''(1)]^2 + [g'(1)]^2 \right\}^{½}, \tag{27}$$

where $\mathrm{Re}_r = r \gamma_i H / \nu_{nf}, i = 1, 2, \ldots,$ is defined as the local Reynolds number.

Nusselt Number

These are defined as

$$Nu_{r_1} = \frac{H q_m}{k_{nf} (T_1 - T_2)} \Big|_{z=0}, \quad \text{where} \quad q_m = -k_{nf} \frac{\partial T}{\partial z} \Big|_{z=0} = -k_{nf} \frac{(T_1 - T_2)}{H} \theta'(0), \quad \text{so} \quad Nu_{r_1} = -\theta'(0), \tag{28}$$

$$Nu_{r_2} = \frac{H q_m}{k_{nf} (T_1 - T_2)} \Big|_{z=H}, \quad \text{where} \quad q_m = -k_{nf} \frac{\partial T}{\partial z} \Big|_{z=H} = -k_{nf} \frac{(T_1 - T_2)}{H} \theta'(1), \quad Nu_{r_2} = -\theta'(1) a. \tag{29}$$

Sherwood Number

These are defined as

$$\begin{aligned} Sh_{r_1} &= \frac{H q_b}{D_B (C_1 - C_2)} \big|_{z=0}, \quad \text{where} \quad q_b = -D_B \frac{\partial C}{\partial z} \big|_{z=0} \\ &= -D_B \frac{(C_1 - C_2)}{H} \phi'(0), \\ &\text{so} \quad Sh_{r_1} = -\phi'(0), \end{aligned} \tag{30}$$

$$\begin{aligned} &Sh_{r_2} = \frac{H q_b}{D_B (C_1 - C_2)} \big|_{z=H}, \quad \text{where} \\ &q_b = -D_B \frac{\partial C}{\partial z} \big|_{z=H} = -D_B \frac{(C_1 - C_2)}{H} \phi'(1), \quad \text{so} \quad Sh_{r_2} = -\phi'(1). \end{aligned} \tag{31}$$

Local Density Motile Flux

These are defined as

$$Sn_{r_1} = \frac{H q_m}{D_m (N_1 - N_2)} \Big|_{z=0}, \quad \text{where} \quad q_m = -D_m \frac{\partial N}{\partial z} \Big|_{z=0} = -D_m \frac{(N_1 - N_2)}{H} \chi'(0), \quad \text{so} \quad Sn_{r_1} = -\chi'(0), \tag{32}$$

$$Sn_{r_2} = \frac{H q_m}{D_m (N_1 - N_2)} \Big|_{z=H}, \quad \text{where} \quad q_m = -D_m \frac{\partial N}{\partial z} \Big|_{z=H} = -D_m \frac{(N_1 - N_2)}{H} \chi'(1), \quad \textit{so} \quad Sn_{r_2} = -\chi'(1). \tag{33}$$

SOLUTION OF THE PROBLEM BY HAM

The current problem is solved with the HAM (homotopy analysis method) software in Mathematica 10 computer-based programing. HAM has been used to solve the problem because this method has the following good aspects.

- Without discretization and linearization of the nonlinear differential equations, this technique is applicable to the system for the best answer.
- This technique is also applicable to those systems which have small or large natural parameters.
- This technique produces the convergent solution of the problem.
- This method is free from a set of base functions and linear operators.

Taking the initial guesses and the linear operators as

$$\begin{aligned} &f_o(\zeta) = s_1 \zeta - (2 s_1 + s_2) \zeta^2 + (s_1 + s_2) \zeta^3,\ g_o(\zeta) = 1 - \zeta + \gamma \zeta,\ \theta_o(\zeta) = 1 - \zeta, \\ &\phi_o(\zeta) = 1 - \zeta,\ \chi_o(\zeta) = 1 - \zeta, \end{aligned} \tag{34}$$

$$L_f = f', \ \mathrm{L}_g = g_\prime, \ L_\theta = \theta'', \ L_\phi = \phi'', \ \text{and} \ L_\chi = \chi'', \tag{35}$$

which satisfy the following properties

$$L_f\left[C_1 + C_2\zeta + C_3\zeta^2 + C_4\zeta^3\right] = 0,\ L_g\left[C_5 + C_6\zeta\right] = 0,\\ L_\theta\left[C_7 + C_8\zeta\right] = 0,\ L_\phi\left[C_9 + C_{10}\zeta\right] = 0,\ L_\chi\left[C_{11} + C_{12}\zeta\right] = 0, \quad (36)$$

where $\{C_i\}_{i=1}^{12}$ are the arbitrary constants.

The zeroth order form of the problems is given as

$$(1-q)L_f\left[f(\zeta,q) - f_o(\zeta)\right] = q\hbar_f N_f\left[f(\zeta,q),\theta(\zeta,q),\phi(\zeta,q),\chi(\zeta,q)\right], \quad (37)$$

$$(1-q)L_g\left[g(\zeta,q) - g_o(\zeta)\right] = q\hbar_g N_g\left[f(\zeta,q),g(\zeta,q)\right], \quad (38)$$

$$(1-q)L_\theta\left[\theta(\zeta,q) - \theta_o(\zeta)\right] = q\hbar_\theta N_\theta\left[f(\zeta,q),g(\zeta,q),\theta(\zeta,p),\phi(\zeta,q)\right], \quad (39)$$

$$(1-q)L_\phi\left[\phi(\zeta,q) - \phi_o(\zeta)\right] = q\hbar_\phi N_\phi\left[f(\zeta,q),\theta(\zeta,q),\phi(\zeta,q)\right], \quad (40)$$

$$(1-q)L_\chi\left[\chi(\zeta,q) - \chi_o(\zeta)\right] = q\hbar_\chi N_\chi\left[f(\zeta,q),\phi(\zeta,q),\chi(\zeta,q)\right], \quad (41)$$

$$f(0,q) = 1, f'(1,q) = 0, f'(0,q) = 1, g(0,q) = 1, g(1,q) = 0,\\ \theta(0,q) = 1, \theta(1,q) = 0,\ \phi(0,q) = 1, \phi(1,q) = 0, \chi(0,q) = 1, \chi(1,q) = 0, \quad (42)$$

where q is an embedding parameter in this case, and $\hbar_f,\hbar_g,\hbar_\theta,\hbar_\phi,\hbar_\chi$ are the nonzero auxiliary parameters. $N_f,N_g,N_\theta,N_\phi,N_\chi$ are the nonlinear operators and can be obtained through **Eqs 17–22** by adopting the procedure in Ref. 47.

For $q = 0$ and $q = 1$, the following form is obtained

$$f(\zeta,0) = f_0(\zeta), \theta(\zeta,0) = \theta_0(\zeta), g(\zeta,0) = g_0(\zeta), \phi(\zeta,0) = \phi_0(\zeta), \chi(\zeta,0) = \chi_0(\zeta),\\ f(\zeta,1) = f(\zeta), \theta(\zeta,1) = \theta(\zeta), \phi(\zeta,1) = \phi(\zeta), \chi(\zeta,1) = \chi(\zeta). \quad (43)$$

Obviously, when q is increased from 0 to 1, then $f(\zeta,q), g(\zeta,q), \theta(\zeta,q), \phi(\zeta,q), \chi(\zeta,q)$ vary from $f_o(\zeta), g_o(\zeta), \theta_o(\zeta), \phi_o(\zeta), \chi_o(\zeta)$ to $f(\zeta), g(\zeta), \theta(\zeta), \phi(\zeta), \chi(\zeta)$. Through Taylor's series expansion, the expressions in the above equations become as

$$f(\zeta,q) = f_o(\zeta) + \sum_{m=1}^{\infty} f_m(\zeta)q^m, f_m(\zeta) = \frac{1}{m!}\frac{\partial^m f(\zeta,q)}{\partial\zeta^m}\Big|_{q=0}, \quad (44)$$

$$g(\zeta,q) = g_o(\zeta) + \sum_{m=1}^{\infty} g_m(\zeta)q^m, g_m(\zeta) = \frac{1}{m!}\frac{\partial^m g(\zeta,q)}{\partial\zeta^m}\Big|_{q=0}, \quad (45)$$

$$\theta(\zeta,q) = \theta_o(\zeta) + \sum_{m=1}^{\infty} \theta_m(\zeta)q^m, \theta_m(\zeta) = \frac{1}{m!}\frac{\partial^m \theta(\zeta,q)}{\partial\zeta^m}\Big|_{q=0}, \quad (46)$$

$$\phi(\zeta,q) = \phi_o(\zeta) + \sum_{m=1}^{\infty} \phi_m(\zeta)q^m, \phi_m(\zeta) = \frac{1}{m!}\frac{\partial^m \phi(\zeta,q)}{\partial\zeta^m}\Big|_{q=0}, \quad (47)$$

$$\chi(\zeta,q) = \chi_o(\zeta) + \sum_{m=1}^{\infty} \chi_m(\zeta)q^m, \chi_m(\zeta) = \frac{1}{m!}\frac{\partial^m \chi(\zeta,q)}{\partial\zeta^m}\Big|_{q=0}. \quad (48)$$

The convergence of the series in **Eqs 44–48** depends strongly upon $\hbar_f,\hbar_g,\hbar_\theta,\hbar_\phi,\hbar_\chi$. By considering that $\hbar_f,\hbar_g,\hbar_\theta,\hbar_\phi,\hbar_\chi$ are selected properly so that the series in **Eqs 44–48** converge at $q = 1$, then these have the following forms

$$f(\zeta) = f_o(\zeta) + \sum_{m=1}^{\infty} f_m(\zeta),\ \ g(\zeta) = g_o(\zeta) + \sum_{m=1}^{\infty} g_m(\zeta),\ \ \theta(\zeta) = \theta_o(\zeta) + \sum_{m=1}^{\infty}\theta_m(\zeta),\\ \phi(\zeta) = \phi_o(\zeta) + \sum_{m=1}^{\infty}\phi_m(\zeta),\ \ \chi(\zeta) = \chi_o(\zeta) + \sum_{m=1}^{\infty}\chi_m(\zeta). \quad (49)$$

The result of the problems at order m deformations can be constructed as follows

$$L_f\left[f_m(\zeta) - \eta_m f_{m-1}(\zeta)\right] = \hbar_f R_f^m(\zeta), \quad (50)$$

$$L_g\left[g_m(\zeta) - \eta_m g_{m-1}(\zeta)\right] = \hbar_g R_g^m(\zeta), \quad (51)$$

$$L_\theta\left[\theta_m(\zeta) - \eta_m \theta_{m-1}(\zeta)\right] = \hbar_\theta R_\theta^m(\zeta), \quad (52)$$

$$L_\phi\left[\phi_m(\zeta) - \eta_m \phi_{m-1}(\zeta)\right] = \hbar_\phi R_\phi^m(\zeta), \quad (53)$$

$$L_\chi\left[\chi_m(\zeta) - \eta_m \chi_{m-1}(\zeta)\right] = \hbar_\chi R_\chi^m(\zeta), \quad (54)$$

$$f_m(0) = f'(0) = f'(1) = 0, g_m(0) = g_m(1) = 0, \theta_m(0) = \theta_m(1) = 0,\\ \phi_m(0) = \phi_m(1) = 0, \chi_m(0) = \chi_m(1) = 0, \quad (55)$$

where $R_f^m(\zeta), R_g^m(\zeta), R_\theta^m(\zeta), R_\phi^m(\zeta)$, and $R_\chi^m(\zeta)$ can be calculated through **Eqs 17–22** with the procedure as in Ref. 47 and $\eta_m = \begin{Bmatrix} 0, & m \le 1 \\ 1, & m > 1 \end{Bmatrix}$.

By solving the m^{th} order deformation problems, the general solutions are

$$f_m(\zeta) = f_m^*(\zeta) + C_1 + C_2\zeta + C_3\zeta^2 + C_4\zeta^3, \quad (56)$$

$$g_m(\zeta) = g_m^*(\zeta) + C_5 + C_6\zeta, \quad (57)$$

$$\theta_m(\zeta) = \theta_m^*(\zeta) + C_7 + C_8\zeta, \quad (58)$$

$$\phi_m(\zeta) = \phi_m^*(\zeta) + C_9 + C_{10}\zeta, \quad (59)$$

$$\chi_m(\zeta) = \chi_m^*(\zeta) + C_{11} + C_{12}\zeta. \quad (60)$$

in which $f_m^*(\zeta), g_m^*(\zeta), \theta_m^*(\zeta), \phi_m^*(\zeta), \chi_m^*(\zeta)$ are the special solutions.

RESULTS AND DISCUSSION

Velocity Profile

Figures 2A–D depict the effect of s_1, s_2, M, and λ on radial velocity profile $f'(\zeta)$. **Figure 2A** reveals that the $f'(\zeta)$ increases at the lower disk by increasing the values of stretching parameter s_1 and decreases near the upper disk. $f'(\zeta)$ takes negative value near the lower disk due to the high stretching and rotation at the upper disk. From **Figure 2B**, it is evident that by increasing stretching parameter s_2, $f'(\zeta)$ enhances near the surface of the upper disk because the stretching rate is greater there. The result is resembled with **Figures 4** and **6** of Hayat et al. [44]. **Figure 2C** shows that $f'(\zeta)$ decreases by increasing magnetic field parameter M. In the hydromagnetic case, the fluid velocity is much smaller than that in the case of hydrodynamic. This is because of the strength of Lorentz force that grows stronger when M increases. Thus, increasing M means increasing the resistive force (Lorentz force) that causes friction between the fluid and the surface, resulting in the reduction of radial velocity. **Figure 2D** shows that $f'(\zeta)$ enhances with the increase in λ values. **Figures 3A,B** show the

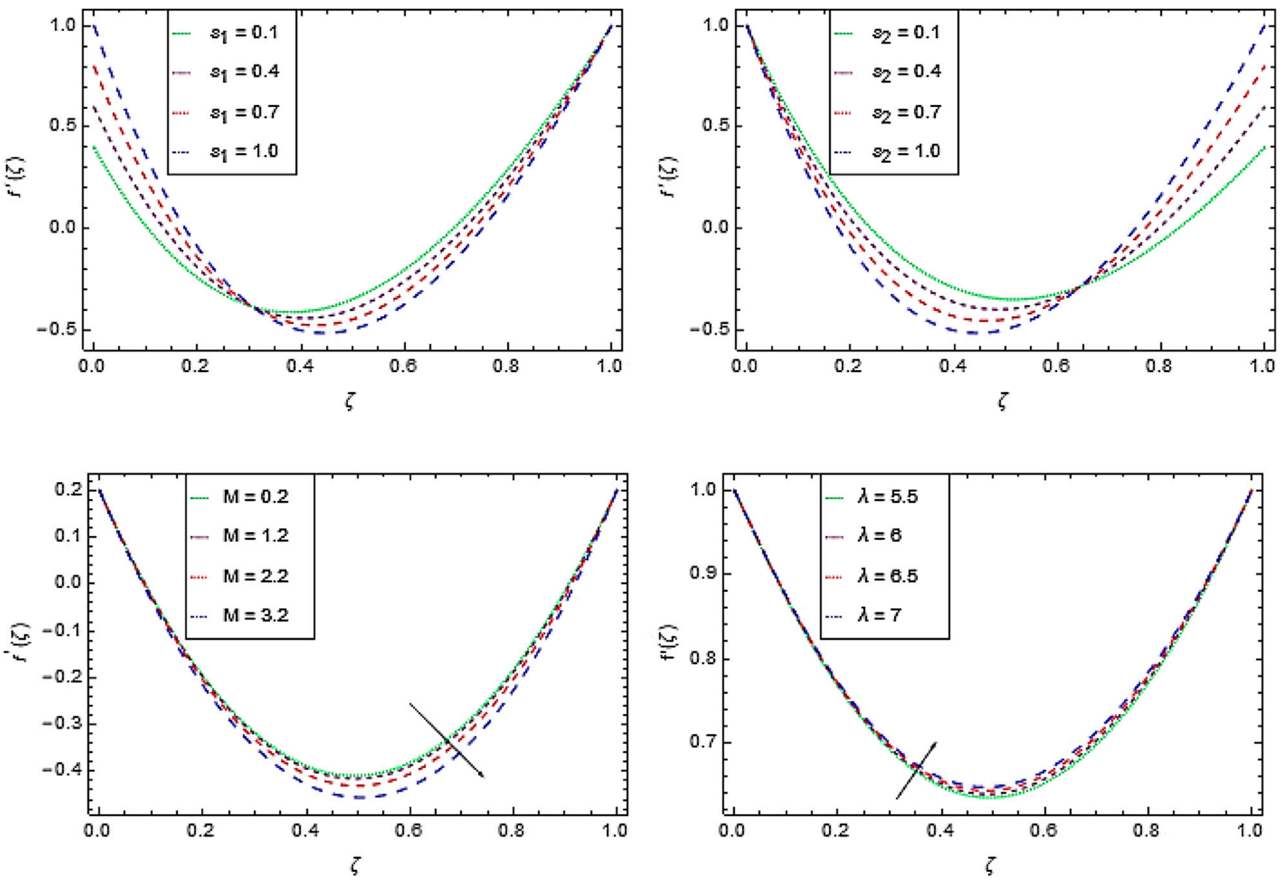

FIGURE 2 | $f'(\zeta)$ as a function of **(A)** s_1, **(B)** s_2, **(C)**, and M **(D)** λ.

effect of bioconvection Rayleigh number Rb and Weissenberg number We on $f'(\zeta)$. **Figure 3A** shows that $f'(\zeta)$ decreases as the convection power of the bioconvection worked against the convection of the buoyancy force. **Figure 3B** shows that by increasing the values of Weissenberg number We, the velocity of Cross nanofluid is decreased, which indicates a thinning liquid shear.

Figure 3C discloses that the rotation paves a long way to enhance the velocity component $g(\varsigma)$. The rotation parameter γ is defined as $\gamma = \gamma_1/\gamma_2$ and has rotatory motion with the essential reliable results. If $\gamma = 0$, then there is no rotation at all and the system remains at rest. $\gamma > 0$ shows that the direction of motion at both of the disks is same, and precisely, $\gamma = 1$ is the same direction and velocity of motion. It is easily understood that rotation directions from both disks are crucial to the motion of the disks. If the two disks rotate within the same direction, the rotation of the fluid in the disks will be at angular velocity. Particularly, the motion of the two disks will be different more likely to be higher in the upper disk, the radial flow is inwardly close to lower disk whereas outwardly close to the upper disk. When the rotation of the lower disk is faster, the liquid flows inward to the lower disk and outward to the upper disk. After all, the two disks attracted to each other, showing that the pressure decreases between the two disks. The plane between the two disks in which the tangential velocity is zero in magnitude is in the opposite direction to each of the disks. Thus, the radial velocity of the fluid is near the plane. Both disks are currently repelling each other, resulting in an increase in pressure. From **Figure 3D**, it is observed that the azimuthal velocity $g(\varsigma)$ is an increasing function of the Hall parameter m. The last term $M/1 + m^2 (g + mf')$ in **Eq. 18** mathematically proves that the velocity $g(\varsigma)$ is increased as the Hall parameter m increases, provided that the magnetic field is strong, that is, the magnetic field parameter M is positive and high enough. It is noted that when there is no magnetic field, that is, if $M = 0$, then the term $M/1 + m^2 (g + mf')$ vanishes consequently and there is no Hall effect.

Pressure Profile

Figures 4A,B depicts the effect of Reynolds number Re and Weissenberg number We on pressure profile $P(\varsigma)$. **Figure 4A** reveals that $P(\varsigma)$ decreases by increasing the values of We. From **Figure 4B**, similar trend is observed by increasing the values of Re. Physically, when the pressure of the flow decays, the flow velocity also decreases, indicating the thinning of the liquid shear.

Temperature Profile

The temperature decreases by increasing the values of thermal conductivity parameter ε as seen in **Figure 5A**. Fluid thermal conductivity is directly related to ε, and because of this, large

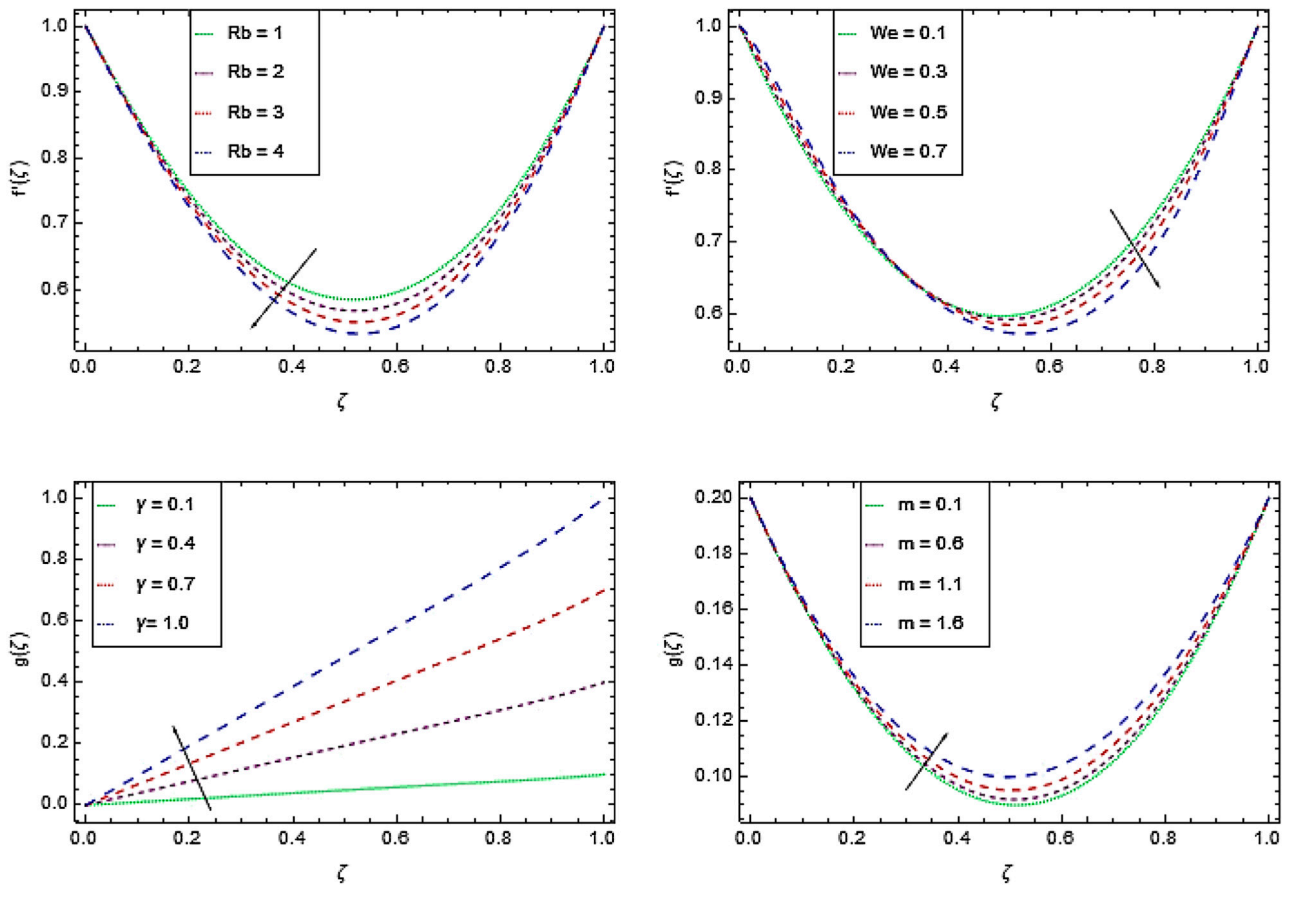

FIGURE 3 | $f'(\zeta)$ as a function of **(A)** *Rb*, **(B)** *We*, and $g(\varsigma)$ as a function of **(C)** γ and **(D)** *m*.

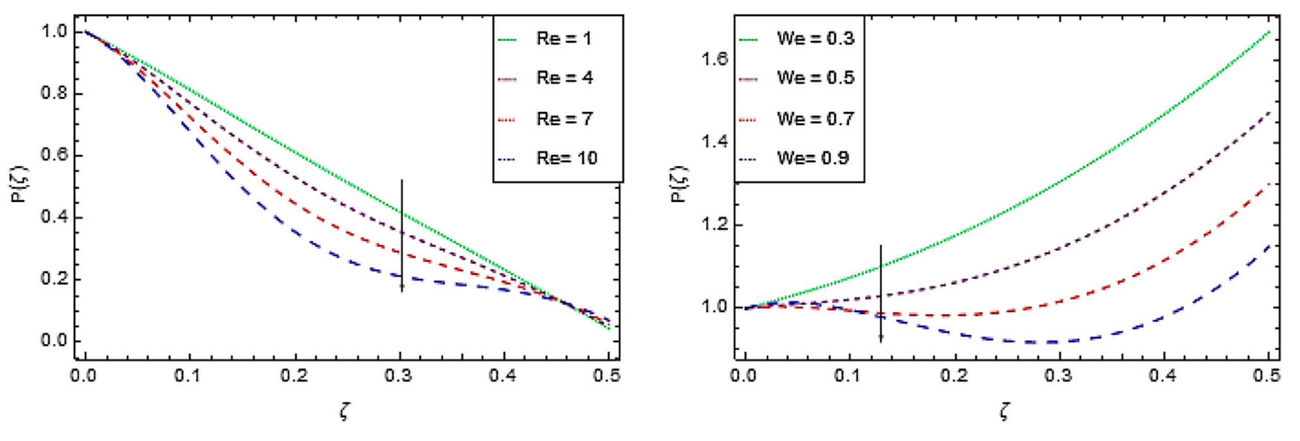

FIGURE 4 | $P(\varsigma)$ as a function of **(A)** Re **(B)** *We*.

heating amount takes place, and then transferred to the fluid through the disk surface due to the increase in temperature $\theta(\zeta)$. **Figure 5B** shows that when Eckert number *Ec* increases, the temperature $\theta(\zeta)$ is increased. *Ec* is the link between the enthalpy flow and the kinetic energy. Work vs. viscous liquid stress is used to convert kinetic energy (KE) into internal energy. The reason is that mechanical energy is converted into thermal energy, so this effect increases the temperature $\theta(\zeta)$ due to heat dissipation. **Figure 5C** demonstrates that Brownian motion parameter *Nb* has the effect of increasing the temperature of the fluid. The fluid particles develop random motion

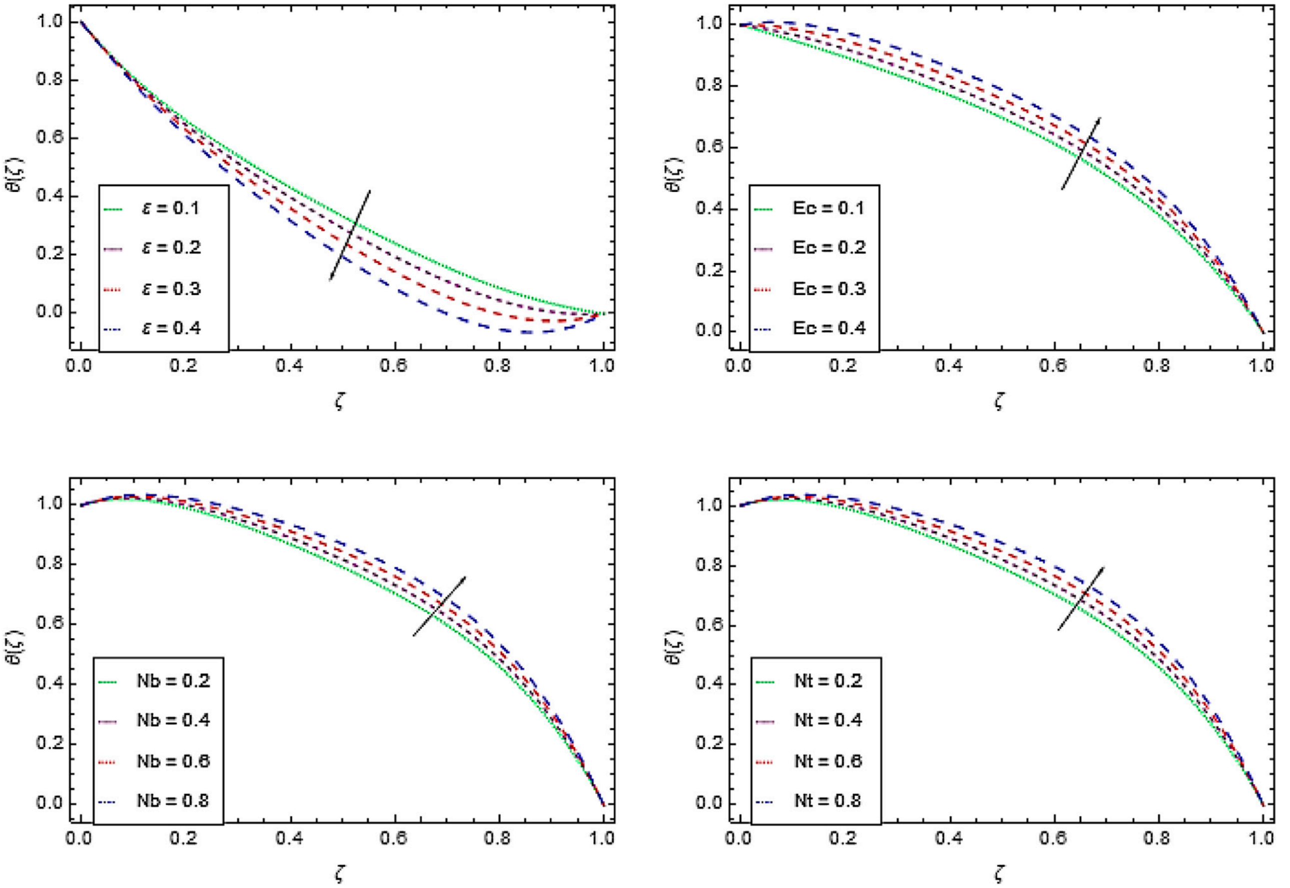

FIGURE 5 | $\theta(\zeta)$ as a function of **(A)** ε, **(B)** *Ec*, **(C)** *Nb*, and **(D)** *Nt*.

as the value of *Nb* increases, leading to a higher temperature distribution $\theta(\zeta)$. There is a significant increase in temperature with higher values of the thermophoresis parameter *Nt* as shown in **Figure 5D**. Essentially, rising in the value of *Nt* means the reinforcement of the thermophoresis forces that tend to transport heat in nanoparticles.

Nanoparticles Concentration Profile

The increase in Arrhenius activation energy E causes the nanoparticles concentration $\phi(\zeta)$ to increase in the boundary layer as shown by **Figure 6A**. Essentially, a larger estimate of the Arrhenius activation energy parameter reduces the value of the modified Arrhenius function that drives the associative chemical reaction. **Figure 6B** shows that the nanoparticles concentration $\phi(\zeta)$ found to be a decreasing function of dimensionless chemical reaction rate σ. As a result, the concentration of fluid decays to a higher estimate of the chemical reaction rate parameter. Larger values of σ are associated with a major devastating chemical reaction that dissolves liquid species quite productively. **Figure 6C** shows that the nanoparticle concentration $\phi(\zeta)$ of fluid is observed to decreasing by a higher estimate of temperature difference parameter δ. The concentration of the nanoparticles decreases by the Brownian motion parameter *Nb* as shown by **Figure 6D**. In addition, it is observed that an increase in *Nb* corresponds to an increase in the rate at which nanoparticles in the base liquid move at different velocity in random directions.

Gyrotactic Microorganism Concentration Profile

Heat treatment makes the system quite fragile and improves production of bioconvection. **Figure 7A** shows that the increment in the motile microorganism's concentration $\chi(\zeta)$ occurs by increasing the values of Lewis number *Le*. That is, the increments in the diffusion of microorganisms can be measured, thus increasing the density and boundary layer thickness of motile microorganism's concentration. **Figure 7B** presents that the increment in the density of the motile microorganisms occurs quickly by increasing the Peclet number *Pe*. This shows a strong relation between the nanoparticles field $\phi(\zeta)$ and the microorganism's field $\chi(\zeta)$.

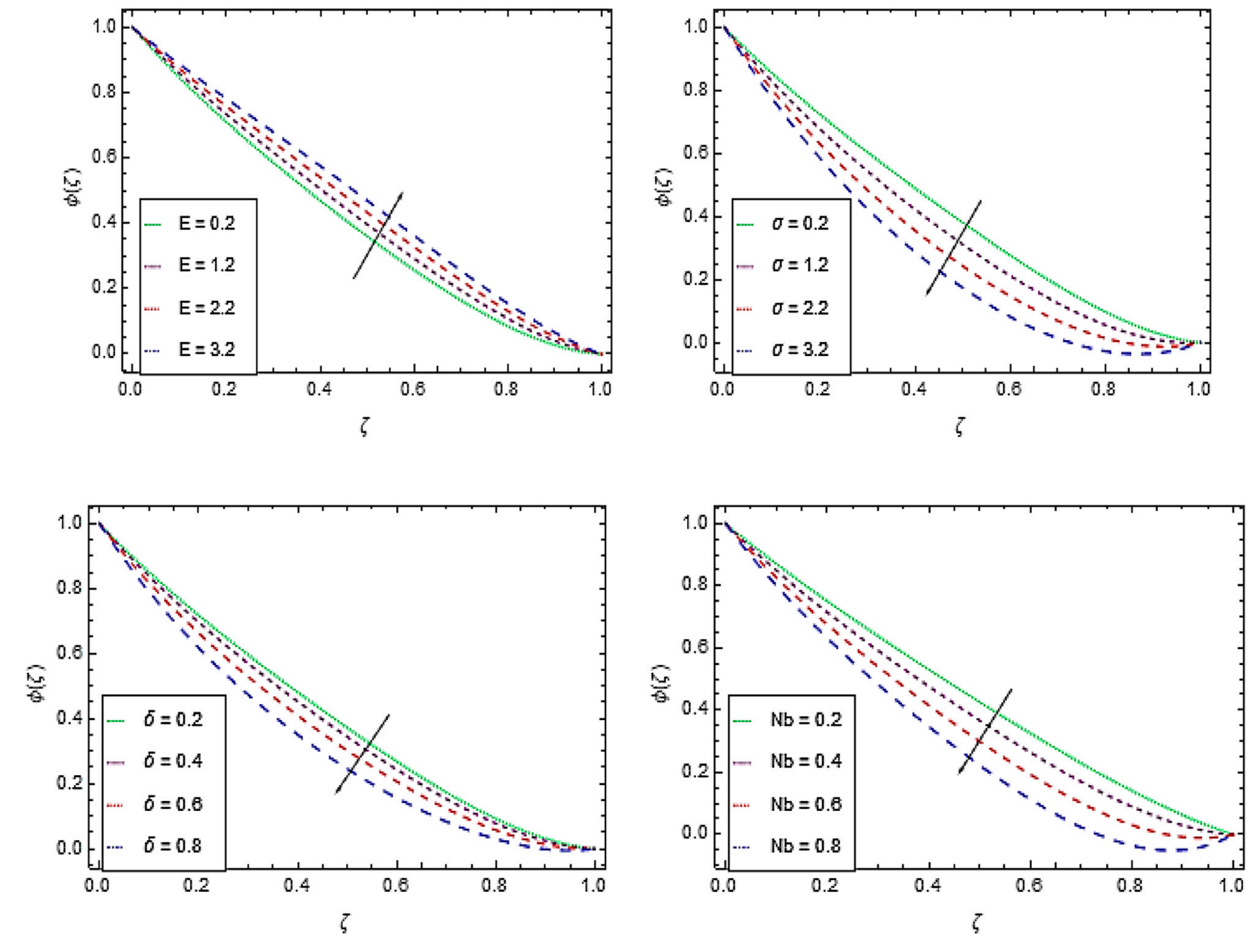

FIGURE 6 | $\phi(\zeta)$ as a function of **(A)** E, **(B)** σ, **(C)** δ, and **(D)** Nb.

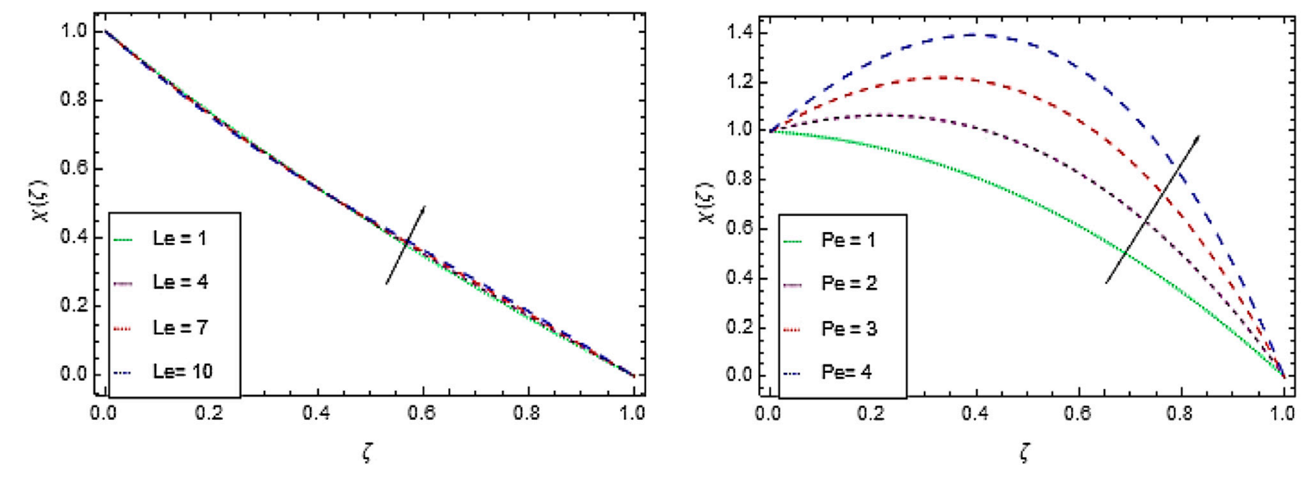

FIGURE 7 | $\chi(\zeta)$ as a function of **(A)** Le and **(B)** Pe.

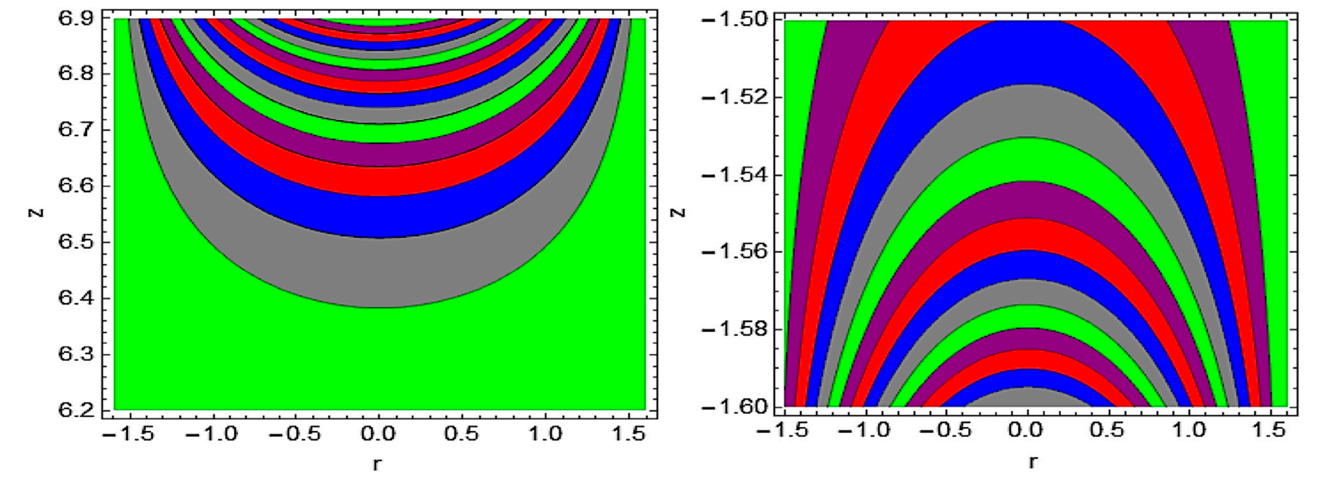

FIGURE 8 | Streamlines for **(A)** $m = 0.2$, $h = -0.1$, for the upper disk **(B)** $h = -0.4$,for the lower disk.

TABLE 1 | Comparison of the present work with the existing literature.

Order of approximation	$-f''(0)$ [44]	$-f''(0)$ Present	$-g'(0)$ [44]	$-g'(0)$ Present
1	1.59936148	1.59936137	0.20487519	0.20487518
2	1.59936096	1.59936085	0.204875663	0.204875662
3	1.59936096	1.59936095	0.204875663	0.204875662
15	1.59936096	1.59936095	0.204875663	0.204875662
20	1.59936096	1.59936095	0.204875663	0.204875662
30	1.59936096	1.59936096	0.204875663	0.204875663
40	1.59936096	1.59936096	0.204875663	0.204875663
50	1.59936096	1.59936096	0.204875663	0.204875663
60	1.59936096	1.59936096	0.204875663	0.204875663

TABLE 2 | Effects of parameters We, λ, γ, m, ε, and M on skin friction coefficients Cf_x.

We	λ	γ	m	ε	M	Cf_{r_1}	Cf_{r_2}
0.5	0.3	1	0.5	0.2	0.5	0.257801	1.73675
1.5						1.61892	2.39153
2.5						1.99648	3.884377
	0.4					0.180041	1.73386
	0.5					0.170060	1.73097
	0.6					0.159468	1.72807
		02				0.189508	1.73675
		03				1.05600	1.77694
		04				1.75464	2.69057
			01			0.541390	1.83803
			1.5			0.666204	1.87336
			02			0.725466	1.88739
				0.4		0.313551	1.82172
				0.6		0.407352	1.90872
				0.8		0.488642	1.99747
					0.7	0.382122	1.76292
					0.9	0.604379	1.78867
					1.1	0.769133	1.81400

TABLE 3 | Effects of parameters Ec, Rd, Nt, Nb, ε, and Pr on local Nusselt number Nu_x.

Ec	Rd	Nt	Nb	ε	Pr	Nu_{r_1}	Nu_{r_2}
0.1	0.3	0.2	0.5	0.3	01	0.653812	2.56824
0.3						0.382616	3.02511
0.5						0.111420	3.48197
	0.6					0.714305	2.29424
	0.9					0.774798	2.02023
	1.2					0.815126	1.74622
		0.4				0.598078	2.89907
		0.6				0.539677	3.24722
		0.8				0.478610	3.61271
			0.7			0.606196	2.86532
			0.9			0.557247	3.17105
			1.1			0.506964	3.48546
				0.5		0.746967	2.35133
				0.7		0.900456	1.99476
				0.9		1.11428	1.49852
					1.3	0.559695	2.96100
					1.6	0.461767	3.36982
					1.9	0.360028	3.79469

TABLE 4 | Effect of parameters σ, E, Nt, Nb, δ, and Sc on local Sherwood number Sh_x.

σ	E	Nt	Nb	δ	Sc	Sh_{r_1}	Sh_{r_2}
0.5	0.5	0.2	0.5	0.2	0.4	1.09124	0.881340
01						1.17102	0.807545
1.5						1.25080	0.733750
	1.5					0.955746	1.01588
	2.5					0.820254	1.15043
	3.5					0.684762	1.28497
		0.4				1.11068	0.818357
		0.6				1.13798	0.739709
		0.8				1.17313	0.645396
			0.7			1.09088	0.889054
			0.9			1.09073	0.893268
			1.1			1.09068	0.895890
				0.3		1.10106	0.876140
				0.4		1.11168	0.870632
				0.5		1.12310	0.864817
					0.8	1.18250	0.758101
					1.2	1.27379	0.630284
					1.6	1.36511	0.497889

Streamlines

The trapping for different values of the Hall parameter m is shown in **Figures 8A** and **8B**. It is observed from these figures that the size of the trapping bolus is higher at the lower disc than in the upper disc for the flow channel.

Validation of the Present Work and Physical Quantities

The comparison between the present work and the previous work is shown in **Table 1**. The results show that there is a close agreement of the present problem. The numerical values of the skin frictions on both the disks are displayed in **Table 2**. The lower disk skin friction is increased with $We, \gamma, m, \varepsilon,$ and M, while the opposite trend is observed for λ. However, the observations on the upper disk were found to be the same with the lower disk. It is examined in **Table 3** that the rate of heat transport on the lower disk is decreased with $Ec, Nt,$ and Nb, while the opposite effect is shown with Rd, Pr, and ε. The observations here are that the rate of heat transport on the upper disk is increased by $Ec, Nt,$ and Nb, while the decreasing effect is shown by Rd, Pr, and ε. The local Sherwood number for the upper disk is decreased with higher values of $\sigma, Nt, \delta,$ and Sc and is increased with E and Nb as shown in **Table 4**. Local density number is enhanced for larger values of Pe, Le, and Re at the lower disk, and opposite trend is observed at the upper disk as shown in **Table 5**.

CONCLUSION

The current work has analyzed the influence of variable thermal conductivity, the Hall current, and activation energy on the flow of double stretchable rotating disks under the theory of radiative Cross nanofluid in the presence of a uniform magnetic field. The fluid functions have been analyzed using graphs and tables explaining the details of the findings in the *Discussion* section. In summary,

TABLE 5 | Effects of parameters Re, Pe, and Le on motile density number Sn_x.

Re	Pe	Le	Sn_{r_1}	Sn_{r_2}
0.5	0.3	0.4	1.11242	0.871653
01			1.13662	0.834806
1.5			1.16909	0.764168
	0.5		1.17625	0.806848
	0.7		1.24178	0.743173
	0.9		1.30901	0.680629
		0.6	1.18636	0.857040
		0.8	1.19646	0.842428
		01	1.20657	0.827818

- The Cross-nanofluid velocity decreases at the boundary layer with the magnetic field parameter M. Radial velocity is proportional to s_1, s_2, λ, and We and inversely proportional to m and Rb.
- The azimuthal velocity g is accelerated by increasing the disk rotation parameter and the Hall effect parameter.
- Pressure profile $P(\varsigma)$ decreases with Re and We.
- The temperature of the Cross nanofluid enhances with increasing the ε, Ec, Nb, Nt parameters.
- The nanofluid concentrations decreases with higher values of δ, σ, Nb while increases with higher values of E.
- Motile gyrotactic microorganism's density increases through larger value of Le and it decreases with Pe and Re.
- The lower disk skin frictions is increased with We, γ, m, ε, and M, while the opposite trend is observed for λ; however, at the upper disk, the case is opposite.
- The rate of heat transport on the lower disk decreases with $Ec, Nt,$ and Nb, while the opposite effects are shown with Rd, Pr, and ε; however, at the upper disk, the case is opposite.
- The local density number is enhanced for the larger values of Pe, Le, and Re at the lower disk, and opposite trend is observed at the upper disk.
- There exists a nice agreement between the present and published work in **Table 1**.

DATA AVAILABILITY STATEMENT

The original contributions presented in the study are included in the article/Supplementary Material, and further inquiries can be directed to the corresponding authors.

AUTHOR CONTRIBUTIONS

NK, AU, UH, ZS, PK, WK, AK, SR, ZU completed the research work.

FUNDING

The research is funded by Petchra Pra Jom Klao Doctoral Scholarship for Ph.D. program of King Mongkut's University of Technology Thonburi (KMUTT) (Grant No. 13/2562) and Theoretical and Computational Science (TaCS) Center. The authors appreciate the financial support allotted by King Mongkut's University of Technology Thonburi through the "KMUTT 55th Anniversary Commemorative Fund." The first author is supported by the Petchra Pra Jom Klao Doctoral Scholarship Academic for PhD studies at KMUTT. This research was accomplished with the help of the Theoretical and Computational Science (TaCS) Center, Faculty of Science, KMUTT.

ACKNOWLEDGMENTS

The authors are obliged to the respectable editor and referees for their important and fruitful comments to enhance the quality of this article. The authors acknowledge the financial support provided by the Center of Excellence in Theoretical and Computational Science (TaCS-CoE), KMUTT. Moreover, this research project is supported by Thailand Science Research and Innovation (TSRI) Basic Research Fund: Fiscal year 2021 under project number 64A306000005.

REFERENCES

1. Cross MM. Rheology of non-newtonian fluids: a new flow equation for pseudoplastic systems. *J Colloid Sci* (1965) 20:417–37. doi:10.1016/0095-8522(65)90022-x
2. Xie J, Jin Y-C. Parameter determination for the cross rheology equation and its application to modeling non-Newtonian flows using the WC-MPS method. *Eng Appl Comput Fluid Mech* (2016) 10:111–29. doi:10.1080/19942060.2015.1104267
3. Manzur M, Khan M, Rahman Mu. Mixed convection heat transfer to cross fluid with thermal radiation: effects of buoyancy assisting and opposing flows. *Int J Mech Sci* (2018) 138–139:515–23. doi:10.1016/j.ijmecsci.2018.02.010
4. Abbas SZ, Khan WA, Sun H, Ali M, Irfan M, Shahzed M, et al. Mathematical modeling and analysis of cross nanofluid flow subjected to entropy generation. *Appl Nanosci* (2020) 10:3149–60. doi:10.1007/s13204-019-01039-9
5. Hayat T, Khan MI, Tamoor M, Waqas M, Alsaedi A. Numerical simulation of heat transfer in MHD stagnation point flow of cross fluid model towards a stretched surface. *Results Phy* (2017) 7:1824–7. doi:10.1016/j.rinp.2017.05.022
6. Naz R, Noor M, Hayat T, Javed M, Alsaedi A. Dynamism of magnetohydrodynamic cross nanofluid with particulars of entropy generation and gyrotactic motile microorganisms. *Int Commun Heat Mass Tran* (2020) 110:104431. doi:10.1016/j.icheatmasstransfer.2019.104431
7. Choi SU, Eastman JA. Enhancing thermal conductivity of fluids with nanoparticles (1995). Report Nos. ANL/MSD/CP-84938; CONF-951135-29. Lemont, IL: Argonne National Lab.
8. Buongiorno J. Convective transport in nanofluids. *J Heat Trans-T ASME* (2006) 128:240–50. doi:10.1115/1.2150834
9. Kuznetsov AV, Nield DA. Natural convective boundary-layer flow of a nanofluid past a vertical plate. *Int J Therm Sci* (2010) 49(2):243–7. doi:10.1016/j.ijthermalsci.2009.07.015
10. Turkyilmazoglu M. Nanofluid flow and heat transfer due to a rotating disk. *Comput Fluids* (2014) 94:139–46. doi:10.1016/j.compfluid.2014.02.009
11. Ahmad L, Khan M, Khan WA. Numerical investigation of magneto-nanoparticles for unsteady 3D generalized Newtonian liquid flow. *Eur Phys J Plus* (2017) 132(9):373. doi:10.1140/epjp/i2017-11658-6
12. Hafeez A, Khan M, Ahmed A, Ahmed J. Rotational flow of Oldroyd-B nanofluid subject to Cattaneo-Christov double diffusion theory. *Appl Math Mech* (2020) 41:1083–94. doi:10.1007/s10483-020-2629-9
13. Khan M, Ahmad L, Gulzar MM. Unsteady Sisko magneto-nanofluid flow with heat absorption and temperature dependent thermal conductivity: a 3D numerical study. *Results Phy* (2018) 8:1092–103. doi:10.1016/j.rinp.2018.01.034
14. Ahmad L, Khan M. Numerical simulation for MHD flow of Sisko nanofluid over a moving curved surface: a revised model. *Microsyst Technol* (2019) 25(6): 2411–28. doi:10.1007/s00542-018-4128-3
15. Khan M, Ahmed J, Sultana F, Sarfraz M. Non-axisymmetric Homann MHD stagnation point flow of Al_2O_3-Cu/water hybrid nanofluid with shape factor impact. *Appl Math Mech* (2020) 41:1125–38. doi:10.1007/s10483-020-2638-6
16. Khan M, Irfan M, Khan WA, Ahmad L. Modeling and simulation for 3D magneto eyring-powell nanomaterial subject to nonlinear thermal radiation and convective heating. *Results Phy* (2017) 7:1899–906. doi:10.1016/j.rinp.2017.06.002
17. Ahmed A, Khan M, Ahmed J. Thermal analysis in swirl motion of Maxwell nanofluid over a rotating circular cylinder. *Appl Math Mech* (2020) 41: 1417–30. doi:10.1007/s10483-020-2643-7
18. Khan M, Ahmad L, Khan WA. Numerically framing the impact of radiation on magnetonanoparticles for 3D Sisko fluid flow. *J Braz Soc Mech Sci Eng* (2017) 39:4475–87. doi:10.1007/s40430-017-0842-5
19. Ahmed J, Khan M, Ahmad L. Radiative heat flux effect in flow of Maxwell nanofluid over a spiraling disk with chemically reaction. *Phys Stat Mech Appl* (2020) 551:123948. doi:10.1016/j.physa.2019.123948
20. Ahmed J, Shahzad A, Farooq A, Kamran M, Khan SUD, Khan SUD. Thermal analysis in swirling flow of titanium dioxide–aluminum oxide water hybrid nanofluid over a rotating cylinder. *J Therm Anal Calorim* (2020):1–11. doi:10.1007/s10973-020-10190-3
21. Ahmed J, Shahzad A, Farooq A, Kamran M, Khan SUD, Khan SUD. Radiative heat transfer in Homann stagnation-point flow of hybrid nanofluid. *Appl Nanosci* (2020) 10:1–10. doi:10.1007/s13204-020-01464-1
22. Li JJ, Xu H, Raees A, Zhao QK. Unsteady mixed bioconvection flow of a nanofluid between two contracting or expanding rotating discs. *Z Naturforsch* (2016) 71:261–72. doi:10.1515/zna-2015-0518
23. Qayyum S, Imtiaz M, Alsaedi A, Hayat T. Analysis of radiation in a suspension of nanoparticles and gyrotactic microorganism for rotating disk of variable thickness. *Chin J Phys* (2018) 56:2404–23. doi:10.1016/j.cjph.2018.06.020
24. Shehzad SA, Reddy MG, Rauf A, Abbas Z. Bioconvection of Maxwell nanofluid under the influence of double diffusive Cattaneo–Christov theories over isolated rotating disk. *Phys Scr* (2020) 95:045207. doi:10.1088/1402-4896/ab5ca7
25. Khan NS, Shah Q, Bhaumik A, Kumam P, Thounthong P, Amiri I. Entropy generation in bioconvection nanofluid flow between two stretchable rotating disks. *Sci Rep* (2020) 10:1–26. doi:10.1038/s41598-020-61172-2
26. Khan NS, Shah Q, Sohail A. Dynamics with Cattaneo–Christov heat and mass flux theory of bioconvection Oldroyd-B nanofluid. *Adv Mech Eng* (2020) 12. doi:10.1177/1687814020930464
27. Khan NS. Mixed convection in mhd second grade nanofluid flow through a porous medium containing nanoparticles and gyrotactic microorganisms with chemical reaction. *Filomat* (2019) 33:4627–53. doi:10.2298/fil1914627k
28. Zuhra S, Khan NS, Islam S. Magnetohydrodynamic second-grade nanofluid flow containing nanoparticles and gyrotactic microorganisms. *Comput Appl Math* (2018) 37:6332–58. doi:10.1007/s40314-018-0683-6
29. Zuhra S, Khan NS, Shah Z, Islam S, Bonyah E. Simulation of bioconvection in the suspension of second grade nanofluid containing nanoparticles and gyrotactic microorganisms. *AIP Adv* (2018) 8:105210. doi:10.1063/1.5054679
30. Palwasha Z, Islam S, Khan NS, Ayaz H. Non-Newtonian nanoliquids thin-film flow through a porous medium with magnetotactic microorganisms. *Appl Nanosci* (2018) 8:1523–44. doi:10.1007/s13204-018-0834-5
31. Arrhenius S. Über die dissociationswärme und den Einfluss der temperatur auf den dissociationsgrad der elektrolyte. *Z Phys Chem* (1889) 4:96–116. doi:10.1515/zpch-1889-0108

32. Bestman AR. Natural convection boundary layer with suction and mass transfer in a porous medium. *Int J Energy Res* (1990) 14:389–96. doi:10.1002/er.4440140403
33. Shahzad M, Sun H, Sultan F, Khan WA, Ali M, Irfan M. Transport of radiative heat transfer in dissipative cross nanofluid flow with entropy generation and activation energy. *Phys Scr* (2019) 94:115224. doi:10.1088/1402-4896/ab2caf
34. Dhlamini M, Kameswaran PK, Sibanda P, Motsa S, Mondal H. Activation energy and binary chemical reaction effects in mixed convective nanofluid flow with convective boundary conditions. *J Comput Des Eng* (2019) 6:149–58. doi:10.1016/j.jcde.2018.07.002
35. Azam M, Xu T, Shakoor A, Khan M. Effects of Arrhenius activation energy in development of covalent bonding in axisymmetric flow of radiative-cross nanofluid. *Int Commun Heat Mass Tran* (2020) 113:104547. doi:10.1016/j.icheatmasstransfer.2020.104547
36. Khan NS, Shah Z, Islam S, Khan I, Alkanhal T, Tlili I. Entropy generation in MHD mixed convection non-newtonian second-grade nanoliquid thin film flow through a porous medium with chemical reaction and stratification. *Entropy* (2019) 21:139. doi:10.3390/e21020139
37. Khan NS, Kumam P, Thounthong P. Second law analysis with effects of Arrhenius activation energy and binary chemical reaction on nanofluid flow. *Sci Rep* (2020) 10:1226–6. doi:10.1038/s41598-020-57802-4
38. Abdelmalek Z, Mahanthesh B, Md Basir MF, Imtiaz M, Mackolil J, Khan NS, et al. Mixed radiated magneto Casson fluid flow with Arrhenius activation energy and Newtonian heating effects: flow and sensitivity analysis. *Alex Eng J* (2020) 59:3991–4011. doi:10.1016/j.aej.2020.07.006
39. Khan NS, Zuhra S, Shah Q. Entropy generation in two phase model for simulating flow and heat transfer of carbon nanotubes between rotating stretchable disks with cubic autocatalysis chemical reaction. *Appl Nanosci* (2019) 9:1797–822. doi:10.1007/s13204-019-01017-1
40. Khan NS, Shah Z, Shutaywi M, Kumam P, Thounthong P. A comprehensive study to the assessment of Arrhenius activation energy and binary chemical reaction in swirling flow. *Sci Rep* (2020) 10:1–21. doi:10.1038/s41598-020-64712-y
41. Kármán TV. Über laminare und turbulente Reibung. *Z Angew Math Mech* (1921) 1:233–52. doi:10.1002/zamm.19210010401
42. Hayat T, Khan MI, Alsaedi A, Khan MI. Joule heating and viscous dissipation in flow of nanomaterial by a rotating disk. *Int Commun Heat Mass Tran* (2017) 89:190–7. doi:10.1016/j.icheatmasstransfer.2017.10.017
43. Yao B, Lian L. A new analysis of the rotationally symmetric flow in the presence of an infinite rotating disk. *Int J Mech Sci* (2018) 136:106–11. doi:10.1016/j.ijmecsci.2017.12.023
44. Hayat T, Qayyum S, Imtiaz M, Alsaedi A. Flow between two stretchable rotating disks with Cattaneo-Christov heat flux model. *Results Phys* (2017) 7:126–33. doi:10.1016/j.rinp.2016.12.007
45. Khan M, Ahmed J, Ahmad L. Chemically reactive and radiative von Kármán swirling flow due to a rotating disk. *Appl Math Mech* (2018) 39:1295–310. doi:10.1007/s10483-018-2368-9
46. Hafeez A, Khan M, Ahmed J. Oldroyd-B fluid flow over a rotating disk subject to Soret–Dufour effects and thermophoresis particle deposition. *Proc IME C J Mech Eng Sci* (2020) 24. doi:10.1177/0954406220946075
47. Liao SJ. *The proposed homotopy analysis technique for the solution of nonlinear problems*. [PhD thesis]. Shanghai (China): Shanghai Jiao Tong University (1992).
48. Liao S-J. An explicit, totally analytic approximate solution for Blasius' viscous flow problems. *Int J Non Lin Mech* (1999) 34:759–78. doi:10.1016/s0020-7462(98)00056-0
49. Shah Z, Gul T, Khan AM, Ali I, Islam S, Husain F. Effects of hall current on steady three-dimensional non-Newtonian nanofluid in a rotating frame with Brownian motion and thermophoresis effects. *J Eng Technol* (2017) 6:e296. doi:10.1115/1.2969753
50. Usman AH, Humphries UW, Kumam P, Shah Z, Thounthong P. Double diffusion non-isothermal thermo-convective flow of couple stress micropolar nanofluid flow in a Hall MHD generator system. *IEEE Access* (2020) 8:78821–35. doi:10.1109/access.2020.2986021
51. Khan NS, Shah Q, Sohail A, Kumam P, Thounthong P, Bhaumik A, et al. Lorentz forces effects on the interactions of nanoparticles in emerging mechanisms with innovative approach. *Symmetry* (2020) 12:1700. doi:10.3390/sym12101700
52. Shah Z, Islam S, Gul T, Bonyah E, Altaf Khan M. The electrical MHD and hall current impact on micropolar nanofluid flow between rotating parallel plates. *Results Phys* (2018) 9:1201–14. doi:10.1016/j.rinp.2018.01.064
53. Usman AH, Shah Z, Humphries UW, Kumam P, Thounthong P. Soret, Dufour, and activation energy effects on double diffusive convective couple stress micropolar nanofluid flow in a Hall MHD generator system. *AIP Adv* (2020) 10:075010. doi:10.1063/5.0014897
54. Zuhra S, Khan NS, Islam S, Nawaz R. Complexiton solutions for complex KdV equation by optimal homotopy asymptotic method. *Filomat* (2019) 33:6195–211. doi:10.2298/fil1919195z
55. Khan NS, Zuhra S, Shah Z, Bonyah E, Khan W, Islam S, et al. Hall current and thermophoresis effects on magnetohydrodynamic mixed convective heat and mass transfer thin film flow. *J Phys Commun.* (2019) 3:035009. doi:10.1088/2399-6528/aaf830
56. Khan NS, Kumam P, Thounthong P. Renewable energy technology for the sustainable development of thermal system with entropy measures. *Int J Heat Mass Tran* (2019) 145:118713. doi:10.1016/j.ijheatmasstransfer.2019.118713
57. Khan NS, Gul T, Islam S, Khan I, Alqahtani A, Alshomrani A. Magnetohydrodynamic nanoliquid thin film sprayed on a stretching cylinder with heat transfer. *Appl Sci* (2017) 7:271. doi:10.3390/app7030271
58. Khan NS. Bioconvection in second grade nanofluid flow containing nanoparticles and gyrotactic microorganisms. *Braz J Phys* (2018) 48:227–41. doi:10.1007/s13538-018-0567-7
59. Khan NS, Gul T, Islam S, Khan W. Thermophoresis and thermal radiation with heat and mass transfer in a magnetohydrodynamic thin film second-grade fluid of variable properties past a stretching sheet. *Eur Phys J Plus* (2017) 132:11. doi:10.1140/epjp/i2017-11277-3
60. Palwasha Z, Khan NS, Shah Z, Islam S, Bonyah E. Study of two-dimensional boundary layer thin film fluid flow with variable thermo-physical properties in three dimensions space. *AIP Adv* (2018) 8:105318. doi:10.1063/1.5053808
61. Khan NS, Gul T, Islam S, Khan A, Shah Z. Brownian motion and thermophoresis effects on MHD mixed convective thin film second-grade nanofluid flow with Hall effect and heat transfer past a stretching sheet. *J Nanofluids* (2017) 6:812–29. doi:10.1166/jon.2017.1383
62. Khan NS, Zuhra S, Shah Z, Bonyah E, Khan W, Islam S. Slip flow of Eyring-Powell nanoliquid film containing graphene nanoparticles. *AIP Adv* (2019) 8:115302. doi:10.1063/1.5055690
63. Khan NS, Gul T, Kumam P, Shah Z, Islam S, Khan W, et al. Influence of inclined magnetic field on Carreau nanoliquid thin film flow and heat transfer with graphene nanoparticles. *Energies* (2019) 12:1459. doi:10.3390/en12081459
64. Khan NS. Study of two dimensional boundary layer flow of a thin film second grade fluid with variable thermo-physical properties in three dimensions space. *Filomat* (2019) 33:5387–405. doi:10.2298/fil1916387k
65. Khan NS, Zuhra S. Boundary layer unsteady flow and heat transfer in a second-grade thin film nanoliquid embedded with graphene nanoparticles past a stretching sheet. *Adv Mech Eng* (2019) 11:1–11. doi:10.1177/1687814019884428
66. Khan NS, Gul T, Islam S, Khan W, Khan I, Ali L. Thin film flow of a second-grade fluid in a porous medium past a stretching sheet with heat transfer. *Alex Eng J* (2017) 57:1019–31.
67. Zuhra S, Khan NS, Alam A, Islam S, Khan A. Buoyancy effects on nanoliquids film flow through a porous medium with gyrotactic microorganisms and cubic autocatalysis chemical reaction. *Adv Mech Eng* (2020) 12:1–17. doi:10.1177/1687814019897510
68. Zuhra S, Khan NS, Khan MA, Islam S, Khan W, Bonyah E. Flow and heat transfer in water based liquid film fluids dispensed with graphene nanoparticles. *Results Phys* (2018) 8:1143–57. doi:10.1016/j.rinp.2018.01.032
69. Liaqat A, Asifa T, Ali R, Islam S, Gul T, Kumam P, et al. A new analytical approach for the research of thin-film flow of magneto hydrodynamic fluid in the presence of thermal conductivity and variable viscosity*ZAMM J Appl Math Mech* (2020):1–13. doi:10.1002/zamm.201900292
70. Liaqat A, Khan NS, Ali R, Islam S, Kumam P, Thounthong P. Novel insights through the computational techniques in unsteady MHD second grade fluid dynamics with oscillatory boundary conditions. *Heat Transf* (2020) 1–23. doi:10.1002/htj.21989
71. Khan NS, Liaqat A, Ali R, Kumam P, Thounthong P. A novel algorithm for the computation of systems containing different types of integral and integro-differential equations. *Heat Transf* (2020) 1–14. doi:10.1002/htj.22018

72. Khan NS, Kumam P, Thounthong P. Computational approach to dynamic systems through similarity measure and homotopy analysis method for the renewable energy. *Crystals* (2020) 1–25. doi:10.3390/cryst10121086
73. Khan NS, Gul T, Khan MA, Bonyah E, Islam S. Mixed convection in gravity-driven thin film non-Newtonian nanofluids flow with gyrotactic microorganisms. *Results Phys* (2017) 7:4033–49. doi:10.1016/j.rinp.2017.10.017
74. Khan NS, Kumam P, Thounthong P. Magnetic field promoted irreversible process of water based nanocomposites with heat and mass transfer flow. *Sci Rep* (2021) 7(1):1692. doi:10.1038/s41598-020-80554-0

Conflict of Interest: The authors declare that the research was conducted in the absence of any commercial or financial relationships that could be construed as a potential conflict of interest

GLOSSARY

$\boldsymbol{u}, \boldsymbol{v}, \boldsymbol{w}$ velocity components

ρ_{nf} density of fluid

ν_{nf} kinematic viscosity

μ_{nf} dynamic viscosity

n power law index

B_o uniform magnetic field strength

$(\rho c_p)_{nf}$ heat capacity of nanofluid

τ ratio of heat capacity

$(\rho c_p)_p$ effective heat capacity

k_{nf} thermal conductivity

σ^* Stefan–Boltzmann constant

D_T thermophoresis effect

T temperature

C concentration

N motile gyrotactic microorganisms

ζ dimensionless variable

f, g dimensionless velocities

θ dimensionless temperature

ϕ dimensionless concentration

χ dimensionless motile microorganisms

P fluid pressure

We Weissenberg number

k_r^2 reaction rate

E Arrhenius activation energydimensionless Arrhenius activation energy

β ratio of viscosities

$\mathbf{Le}$ Lewis number

$\mathbf{Pe}$ Peclet number

γ rotation parameter

$\mathbf{s_1}$ lower disk rotation rate

$\mathbf{s_2}$ upper disk rotation rate

k^* mean absorption coefficient

Γ time material constant

D_B Brownian motion

$\mathbf{Pr}$ Prandtl number

M magnetic parameter

Nr Buoyancy ratio parameter

λ mixed convection parameter

Rb Rayleigh number bioconvection

Nb Brownian motion parameter

Nt thermophoresis parameter

Ec Eckert number

Sc Schmidt number

σ dimensionless chemical reaction rate

E Arrhenius activation energydimensionless Arrhenius activation energy

δ temperature difference parameter

N_δ microorganisms concentration variance parameter

β_1 dimensionless parameter 1

β_2 dimensionless parameter 2

Rd thermal radiation parameter

ε thermal conductivity parameter

$K(\mathbf{T})$ variable thermal conductivity

τ_w wall shear stress

q_w wall heat flux

Cf_x skin friction coefficient

Nu_x local Nusselt number

Sh_x Sherwood number

Sn_x local density number

Re_x local Reynolds number